frontiers | Frontiers in Energy Research

TYPE Original Research
PUBLISHED 17 March 2025
DOI 10.3389/fenrg.2025.1511271

OPEN ACCESS

EDITED BY
Sumanta Sahoo,
Yeungnam University, Republic of Korea

REVIEWED BY
Chuanyu Sun,
University of Padua, Italy
Amin Mohammadpour,
Shiraz University of Medical Sciences, Iran

*CORRESPONDENCE
Anshu Sharma,
anshushsharda@gmail.com

RECEIVED 14 October 2024
ACCEPTED 26 February 2025
PUBLISHED 17 March 2025

CITATION
Manisha, Qaeemy MT, Dhanda M, Lata S, Kumar H and Sharma A (2025) Optimization of Nb_2O_5/g-C_3N_4/PPy as an electrode material for prevailing electrochemical performance. *Front. Energy Res.* 13:1511271. doi: 10.3389/fenrg.2025.1511271

Optimization of Nb_2O_5/g-C_3N_4/PPy as an electrode material for prevailing electrochemical performance

Manisha[1], M. Taqi Qaeemy[1], Monika Dhanda[2], Suman Lata[2], Harish Kumar[3] and Anshu Sharma[4]*

[1]Department of Physics and Astrophysics, School of Basic Sciences, Central University of Haryana, Mahendragarh, India, [2]Department of Chemistry, Deenbandhu Chhotu Ram University of Science and Technology, Murthal, Haryana, India, [3]Department of Chemistry, School of Basic Sciences, Central University of Haryana, Mahendragarh, India, [4]Department of Applied Sciences and Humanities, School of Engineering and Technology, Central University of Haryana, Mahendragarh, India

The use of a ternary composite employing carbon material, polymer and metal oxide can effectively increase the performance of an electrode material used in Supercapacitors. Herein, we have facilely synthesized ternary composites of Nb_2O_5/g-C_3N_4/PPy (NGP) via in-situ polymerization reaction by systematically varying the amount of niobium pentoxide. The structural and morphological analysis of samples were examined through XRD, TGA, FESEM and BET, confirming a specific surface area of 68.936 m^2/g for NGP composite. Nb_2O_5 nanoparticles prevent the restacking of g-C_3N_4 sheets and PPy form a spongy globular morphology around this structure resulting in enhanced electrochemical performance. Electrochemical assessments of the optimized composite, including CV, GCD, and EIS, revealed a specific capacitance of 1,290.15 F/g at 2 mV/s in 1 M H_2SO_4, with an energy density of 75.25 W h/kg at a power density of 450.01 W/kg, demonstrating the efficacy of the ternary composite strategy in advancing supercapacitor electrode properties. After 5000 CV cycles and 1000 GCD cycles, the electrode retained a specific capacitance of 95% and 91% of its initial value, respectively.

KEYWORDS

supercapacitors, three-electrode setup, polymer composite, ternary composite, specific surface area, specific capacitance, power/energy density

Highlights

- The spongy globular morphology of NGP composites was facilely synthesized via chemical in-situ polymerization resulting in specific surface area of 68.936 m^2/g.
- The kinetics of electrode-electrolyte interaction was examined by obtaining CV curve at varied scan rates.
- The maximum value of specific capacitance for NGP0.4 composite was evaluated to be 1,290.15 F/g at 2 mV/s.

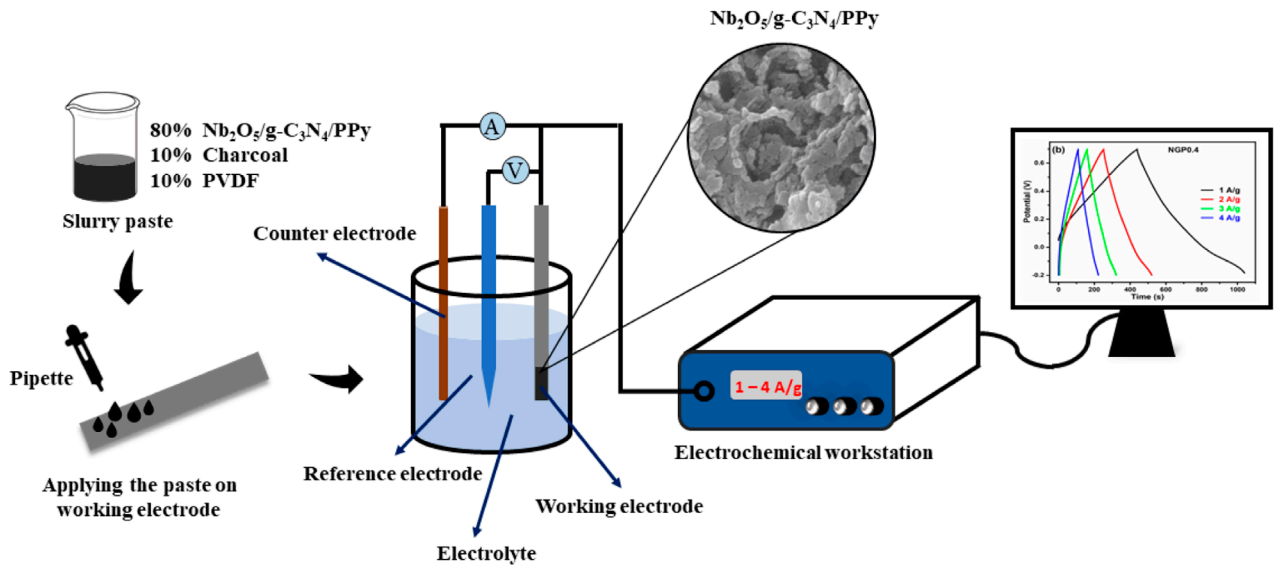

GRAPHICAL ABSTRACT

Introduction

As the global population continues to advance, the demand for energy is also increasing which necessitates the development of efficient energy conversion and storage devices (Mao et al., 2021). About one-seventh of the world's primary energy is sourced from renewable energy but renewable energy sources are location specific and thus limiting its utilization in context of global decarbonization (Huan et al., 2024). Among the storage devices, batteries are leading the way, however, in their conventional form, they suffer from low power density and raises environmental concerns which makes them less reliable for future generations (Ray and Saruhan 2021). In contrast, Supercapacitors are emerging as a key player in this race because of their high power density, environmental friendliness and non hazardous nature. Nevertheless, their low energy density is a major hurdle which needs attention (Pan et al., 2024; Pore et al., 2021).

The energy density of Supercapacitors is primarily influenced by the choice of electrode material, electrolyte and current collector (Dhanda et al., 2022a). From the literature, it is evident that the selection of electrode material has significant impact on the specific capacitance and consequently energy density of Supercapacitor (Shimoga et al., 2021; Moreno et al., 2020). Electrode material consisting of metal oxides, conductive polymers and carbon derivatives have been rigorously used in Supercapacitors because of their charge storing mechanism which exhibit properties of both Electric Double layer and pseudocapacitive, resulting in overall increase of capacitance (Dhanda et al., 2022b; Arora et al., 2022a). In principle, metal oxides based electrode materials have high specific capacitance but their high cost, low conductivity and toxicity to the environment limits their direct use (Mustaqeem et al., 2022). On the other hand, conductive polymers have also high specific capacitance but have low cyclic stability. Conversely, carbon materials possess good cyclic stability but lower values of specific capacitance (Dhanda et al., 2022c). Thus, a lot of research is being conducted on the ternary composite consisting of carbon materials, conductive polymers and metal oxides where their synergistic effect leads to a better energy storage material (Vandana et al., 2022; Ishaq et al., 2019; Moyseowicz et al., 2017; Zhang et al., 2017).

For instance, polypyrrole (PPy) has been chosen over other conducting polymers like polyaniline (PANI) and polythiophene (PEDOT) because of its better electrical conductivity. For instance, the synthesis of PPy can be done in aqueous media while synthesis of PANI requires strong acidic medium which can lead to handling and disposal challenges. In addition, PEDOT has lower charge storage than PPy and PANI. (Huang et al., 2016; Choudhary et al., 2020). Graphitic carbon nitride (g-C_3N_4), a 2D material having structure similar to that of graphene, possesses an optical band gap of 2.7eV and have high specific surface area making it a preferable material for electric double layer capacitance (Paul et al., 2019; Manisha et al., 2025). Niobium pentoxide (Nb_2O_5) despite its low electrical conductivity (3×10^{-6} S cm^{-1}) supports redox reaction due to its variable oxidation states, thus results in a higher value of specific capacitance (Shen et al., 2021). Murugan et al. synthesized the composite of reduced graphene oxide with niobium pentoxide by hydrothermal reaction (Murugan et al., 2016). Vicentini et al. has developed a ternary composite of niobium pentoxide with Multi–walled carbon nanotude (MWCNT) and activated carbon (AC) via electrodeposition (Vicentini et al., 2019). Lim et al. synthesized a hybrid supercapacitor based on Nb_2O_5 and carbon as an anode (Lim et al., 2014). The specific capacitance observed in these literature is lesser than 400 F g^{-1} but power density is significantly higher since the operating potential window is higher than 1 V (Qin et al., 2020).

In this research, we have synthesized a ternary composite of Nb_2O_5/g-C_3N_4/PPy (NGP) via facile one step in-situ polymerization reaction and evaluated its performance in aqueous electrolyte. The operating potential window was

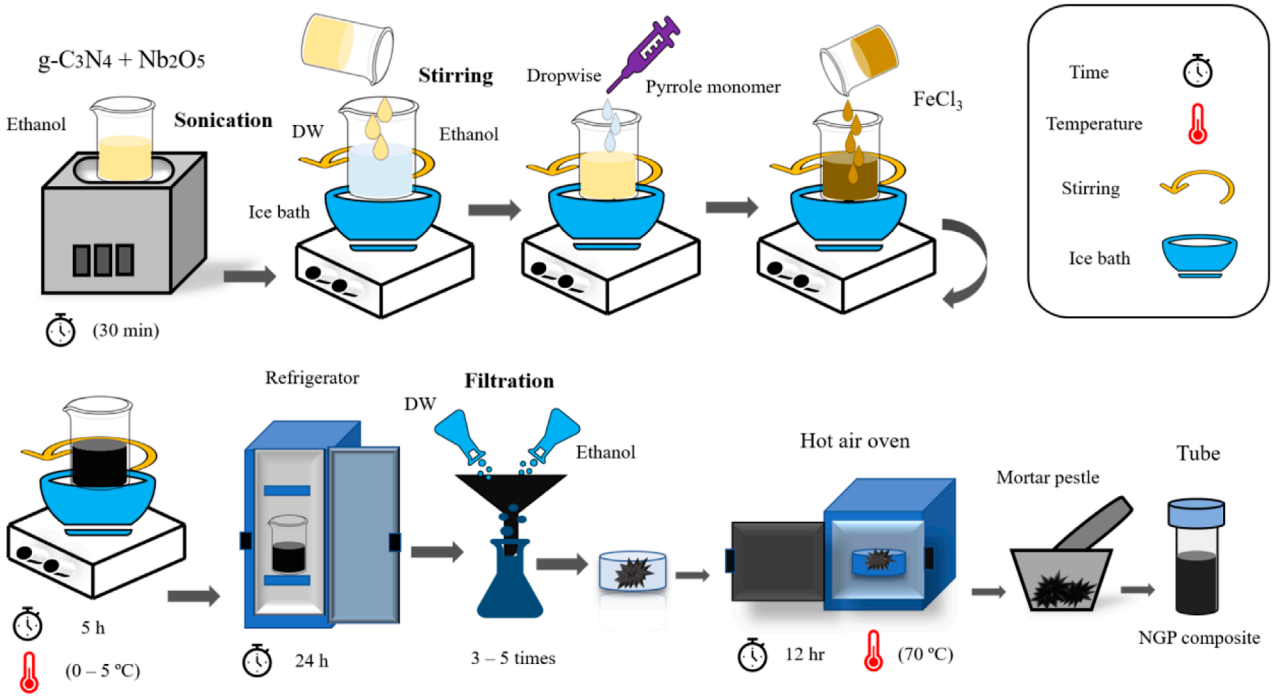

FIGURE 1
Schematic illustration of the synthesis of NGP composites.

TABLE 1 Composition of precursors in NGP composite.

Nb_2O_5 (g)	g-C_3N_4 (g)	Pyrrole (mL)	Material
0.2	0.4	0.5	NGP0.2
0.3	0.4	0.5	NGP0.3
0.4	0.4	0.5	NGP0.4
0.5	0.4	0.5	NGP0.5

maintained below 1 V so as to not include the specific capacitance due to electrolysis of water. This innovative approach aims to enhance the overall performance of electrode material by leveraging the synergistic effect of composite material. Niobium pentoxide is expected to provide high capacity and redox activity, graphitic carbon nitride enhances the conductivity and stability while the addition of Polypyrrole further strengthens the integrity and flexibility of composite.

Experimental details

Chemicals

All the chemicals used during synthesis were of analytical grade. Niobium pentoxide (Nb_2O_5, 99.9%) and polyvinylidene fluoride (PVDF, 99.9%) were purchased from Sigma Aldrich. Ferric chloride (99%) and pyrrole (99%) were obtained through chemical drug house (CDH), Urea (99%) and dimethylformamide (DMF, AR) was bought from Thermo Fischer Scientific. Distilled water was used during the synthesis and cleaning.

Synthesis of Nb_2O_5/g-C_3N_4/PPy

The ternary composite Nb_2O_5/g-C_3N_4/PPy (NGP) was synthesized via an in-situ polymerization reaction as shown in Figure 1. Initially, g-C_3N_4, which was obtained by calcination of urea at 550°C as described in prior literature (Manisha et al., 2023), was combined with niobium pentoxide (Nb_2O_5). These two components were dispersed in 30 mL ethanol and subjected to ultrasonication for 30 min to ensure thorough mixing. This was then transferred to an ice bath containing the solution of ethanol and distilled water. Subsequently, 0.5 mL of pyrrole was introduced to this. After proper mixing, a freshly prepared 0.1 M ferric chloride solution was added to the solution to initiate the polymerization reaction. Then, the solution was kept on stirring for 5 h while maintaining the temperature between 0 and 5°C. Following this, the mixture was stored in refrigerator overnight and then filtered through whatmann filter paper (Arora et al., 2022b). The precipitates were properly washed with ethanol and distilled water to remove the impurities and then dried in a hot air oven at 60°C for 12 h. The resulting material was grounded well with mortar and pestle to obtain black powder. Table 1 depicts the ratio of different materials in final composite.

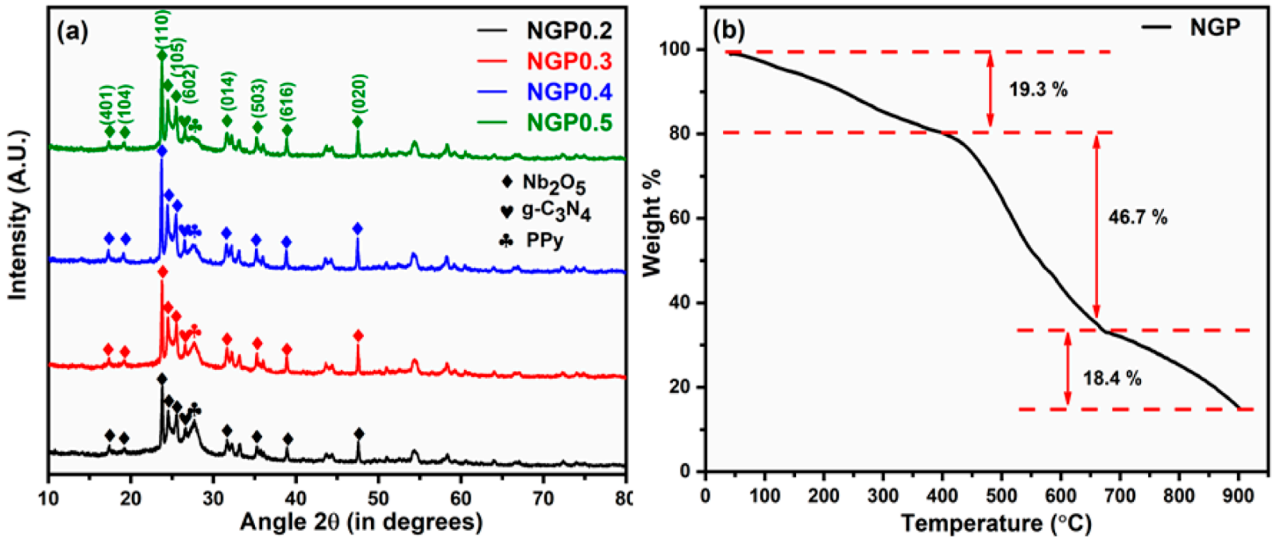

FIGURE 2
(a) XRD pattern of NGP0.2, NGP0.3, NGP0.4 and NGP0.5 **(b)** TGA graph of NGP composite.

Characterization techniques

To verify the successful synthesis of samples, X-ray Diffraction (XRD) was conducted using a Rigaku Smart Lab setup with X-ray of wavelength 1.54 A^0 at a scan rate of 2^0/min. The morphology of synthesized samples was further performed by Zeiss GeminiSEM 500 utilizing the technique Field Emission Scanning Electron Microscopy (FESEM). Thermal stability of samples was analyzed by Thermo Gravimetric Analysis (TGA) performed on TGA HiRes1000 in nitrogen atmosphere at a heating rate of 4°C/min. The specific surface area and pore size analysis was performed through Brunauer–Emmett–Teller (BET) by Nova touch LX4 Quanta chrome, Anton PAAR, 2021 at 77 K in nitrogen atmosphere after degassing the sample at 60°C for 24h.

Electrochemical measurements

After confirming the proper synthesis of samples, electrochemical measurements were performed on Biologic electrochemical workstation VSP300. For electrochemical testing, slurry of sample was prepared by dispersing the 80 mg active material, 10 mg acetylene black and 10 mg PVDF in DMF solvent. This slurry was pasted on a high density graphite sheet using drop casting technique and was kept in hot air oven overnight (Sayed et al., 2020). The weight of the loaded mass was calculated by subtracting the weight of bare electrode from the weight of pasted electrode and found to be approximately 1 mg. To assess the capability of this material as an electrode material for supercapacitors, three electrode measurements were performed by taking this as a working electrode, Ag/AgCl as reference electrode and platinum wire as counter electrode using 1 M H_2SO_4 as an electrolyte. The specific capacitance, energy density and power density of material was evaluated by Cyclic Voltammetry (CV), Galvanostatic Charge Discharge (GCD) by employing the following equations (Jhanjhariya and Lata 2024)

$$C_v = \frac{\int IdV}{ms \triangle V} \quad (1)$$

$$C_d = \frac{I \times \triangle t}{m \times \triangle V} \quad (2)$$

$$E = \frac{1}{2 \times 3.6} \times C_d \times \triangle V^2 \quad (3)$$

$$P = 3600 \times \frac{E}{\triangle t} \quad (4)$$

Where C_v and C_d represents the specific capacitance in F/g from CV and GCD respectively, I is the current in mA, s is the scan rate of CV in mV/s, $\triangle V$ and $\triangle t$ demonstrates the operating potential window in V and discharging time in seconds from GCD data, E and P shows the energy density and power density in W h/kg and W/kg respectively, obtained from GCD data.

Results and discussion

Figure 2a presents the XRD pattern of NGP0.2, NGP0.3, NGP0.4 and NGP0.5, obtained in 2θ range from 10^0 to 80^0. The XRD pattern corresponds well with the JCPDS PDF No. 01–071-0,005 depicting the pseudohexagonal phase of Nb_2O_5 (Hu et al., 2020). A small peak at 27^0 denotes the (002) plane of g-C_3N_4 indicative of its layered structure, alongside a broad peak is observed at 27.7^0 indicating the presence of amorphous PPy (Lü et al., 2022; Paul et al., 2022). As the concentration of Nb_2O_5 increased in the composites, PPy peak get diminishes and the intensity of Nb_2O_5 peaks increases suggesting its interaction during synthesis. This behavior demonstrates the successful incorporation of Nb_2O_5 into the composites, confirming their proper synthesis.

The thermal stability and phase transitions of NGP composite during annealing was examined by performing TGA over a

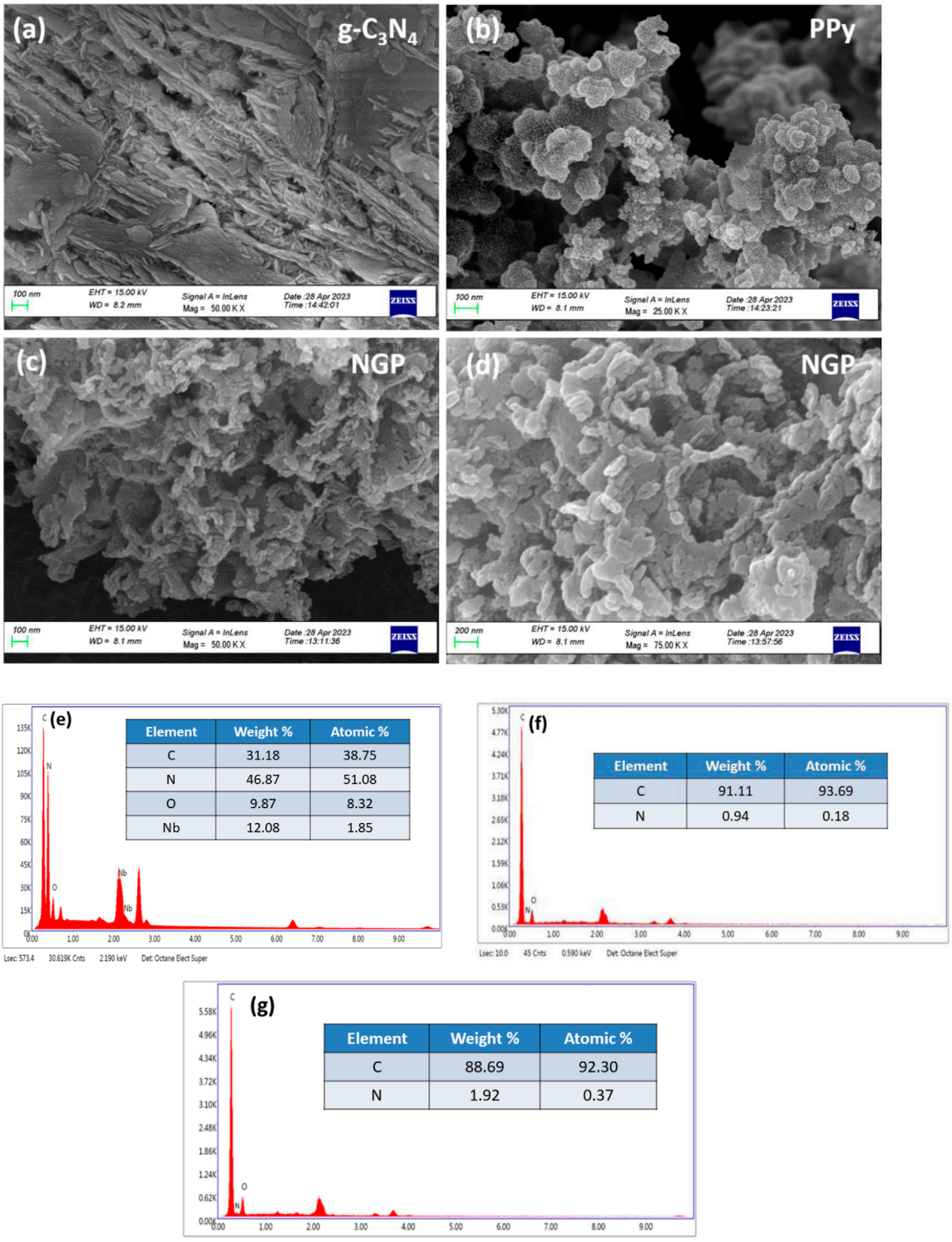

FIGURE 3
(a) FESEM image of g-C_3N_4 at 50K **(b)** FESEM image of PPy at 25K **(c)** FESEM image of NGP composite at 50K **(d)** FESEM image of NGP composite at 75K **(e)** EDX spectra of NGP composite **(f)** EDX spectra of PPy **(g)** EDX spectra of g-C_3N_4.

temperature range from 40°C to 900°C. Figure 2b displays the TGA curve of NGP composite demonstrating a two stage weight loss process. An initial weight loss of approximately 20% was observed up to 400°C which might be attributed to the loss of water molecules and other volatile impurities present in the material. During this stage, decomposition of PPy chain also begins, indicated by a linear weight loss (Sun et al., 2019). Between 400°C and 650°C, a substantial weight loss was observed due to the complete

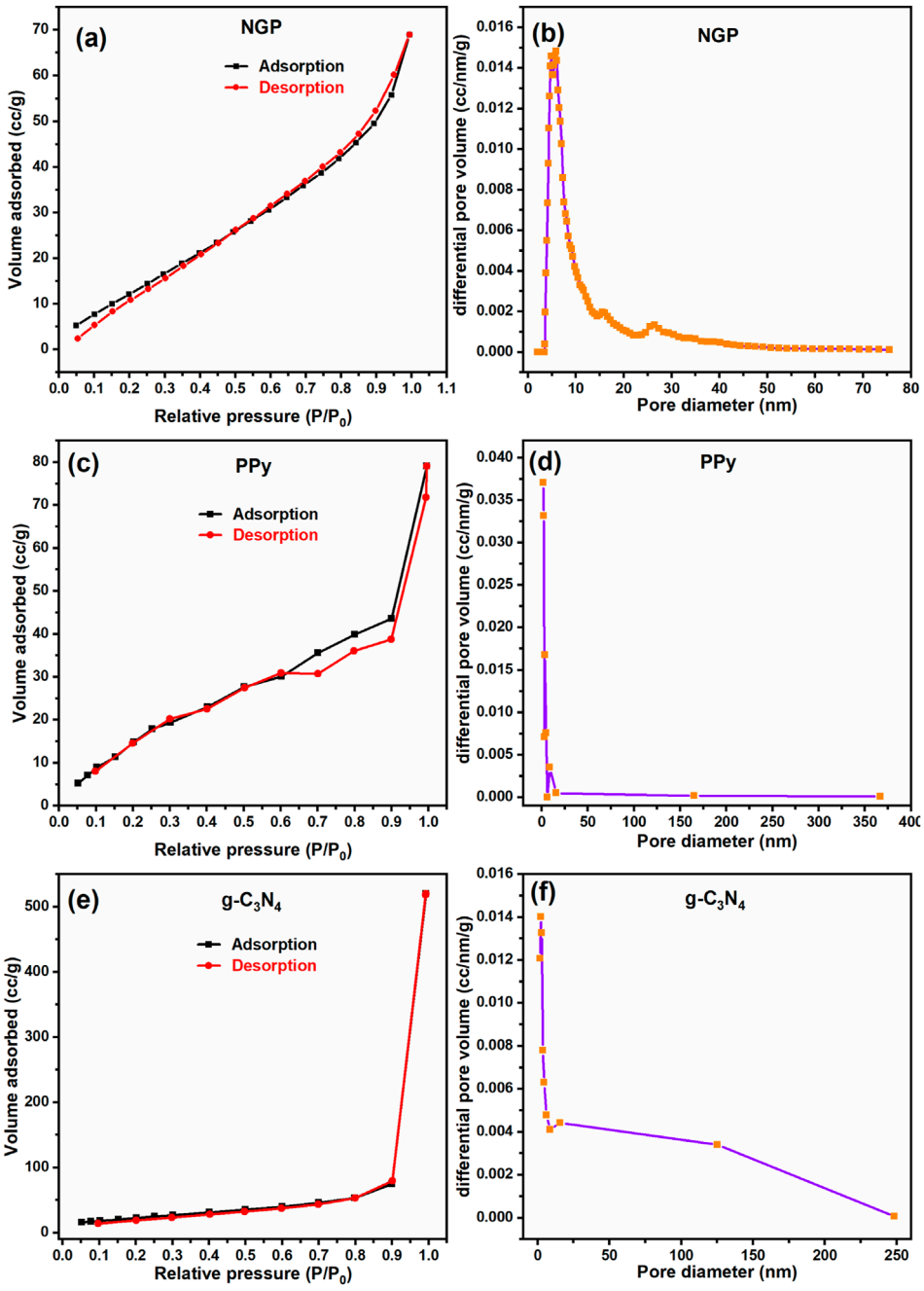

FIGURE 4
Adsorption–desorption isotherm and the distribution of pore diameter with differential pore volume for **(a, b)** NGP composite **(c, d)** PPy **(e, f)** g-C_3N_4.

TABLE 2 Distribution of pore surface area, pore volume and pore diameter.

Material	Pore surface area (m^2/g)	Pore volume (cc/g)	Pore diameter (nm)
g-C_3N_4	85.896	0.817	2.325
PPy	82.071	0.145	1.809
NGP	68.936	0.105	3.077

decomposition of PPy chain and g-C_3N_4 also starts decomposing into carbon dioxide and nitrogen gases (Ullah et al., 2022). From 650°C to 900°C, the weight loss is about 18% showing the complete decomposition of g-C_3N_4 but the material is not completely decomposed which means that at higher temperatures, Nb_2O_5 changes its phase from pseudohexagonal to a more stable structure orthorhombic which matches with the literature (Li et al., 2016).

Figures 3a–d presents the FESEM images of g-C_3N_4, PPy and NGP composite. g-C_3N_4 has a characteristic sheet like structure which ensures structural integrity while PPy has spongy globular

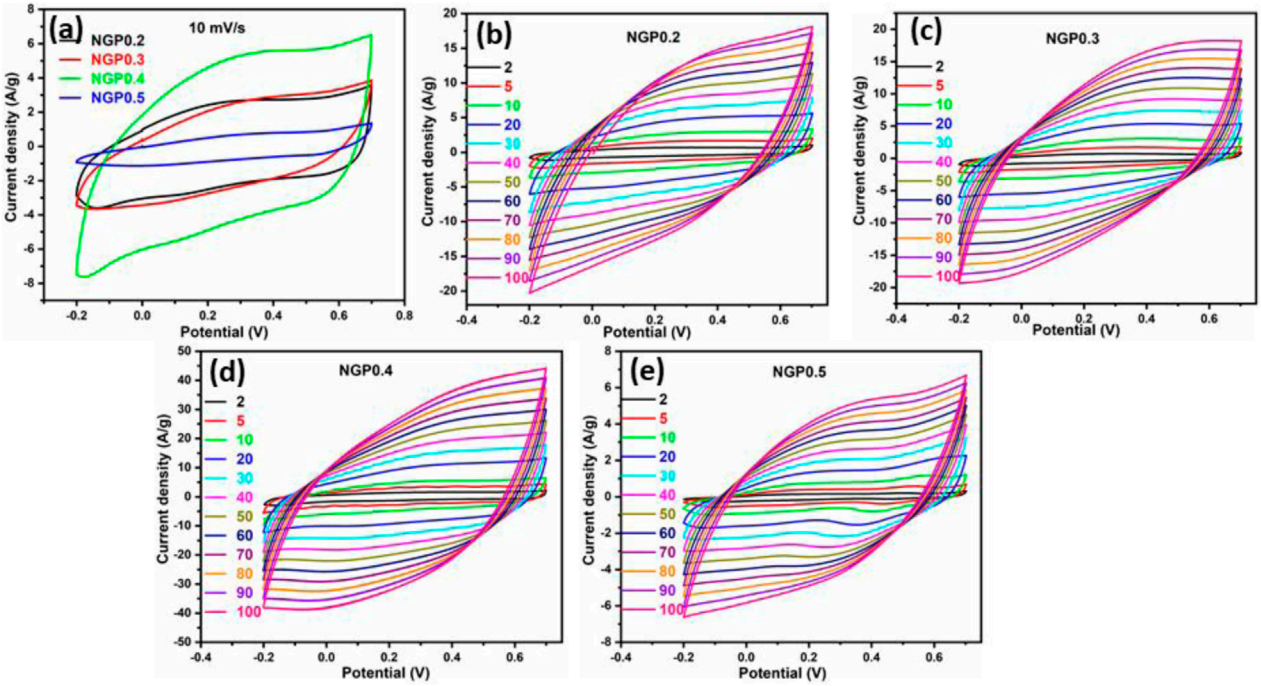

FIGURE 5
(a) Cyclic voltammetry curve of NGP0.2, NGP0.3, NGP0.4 and NGP0.5 at 10 mV/s **(b–e)** CV curve for NGP0.2, NGP0.3, NGP0.4 and NGP0.5 composite at varying scan rate from 2 mV/s to 100 mV/s.

TABLE 3 Specific capacitance of NGP composites at a scan rate of 10 mV/s.

Material	Specific capacitance (F/g)
NGP0.2	446.79
NGP0.3	455.64
NGP0.4	**897.81**
NGP0.5	138.26

The bold value represents optimized NGP composite with maximum specific capacitance.

TABLE 4 Variation of specific capacitance with scan rate for NGP0.4 composite.

Scan rate (mV/s)	Specific capacitance (F/g)			
	NGP0.2	NGP0.3	NGP0.4	NGP0.5
2	554.20	557.13	**1,290.15**	145.38
5	501.98	508.67	1,086.87	144.22
10	446.79	455.64	897.81	138.26
20	386.43	395.82	843.51	127.10
30	357.47	358.41	774.24	118.78
40	329.56	330.48	723.49	111.68
50	306.87	308.68	681.85	105.53
60	288.05	290.68	647.88	100.22
70	271.05	275.51	618.61	95.34
80	256.59	262.29	591.24	91.17
90	243.34	250.65	567.46	87.28
100	229.22	240.14	545.42	83.83

The bold value represents optimized NGP composite with maximum specific capacitance.

morphology facilitating faster electron and ion transport. Upon examining the morphology of NGP composite, it is evident that niobium pentoxide nanoparticles are encapsulated on sheet like structures of g-C_3N_4 around which PPy has formed a spongy network resulting in an interconnected morphology, which significantly enhances the interaction between composite's constituents. This enhanced interaction between Nb_2O_5, g-C_3N_4 and PPy provides a synergistic effect which helps in efficient charge storage. Figures 3e–g represents the elemental composition of different elements in the NGP composite, PPy and g-C_3N_4, illustrating the presence and proportion of different elements. The presence of oxygen in PPy and g-C_3N_4 might be due to the absorption of moisture. Hydrogen is not reported in EDX analysis because energy levels of characteristic X-rays for hydrogen are extremely low (below 0.01 keV) and hence not detected by detector.

Figure 4 displays the adsorption-desorption isotherm of g-C_3N_4, PPy and NGP composite which was obtained in the relative pressure range from 0 to 1. The isotherms exhibit type IV profile with negligible hysteresis depicting that mesopores are uniform and the adsorption-desorption is nearly reversible (Pathak et al.,

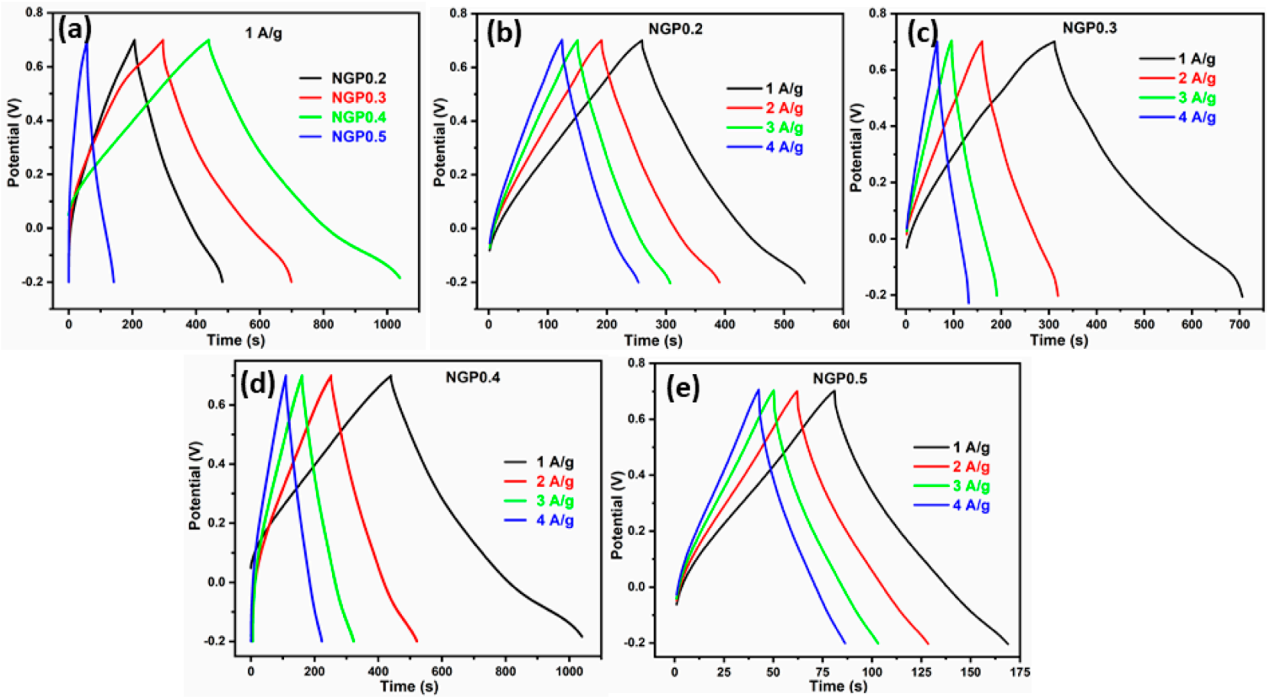

FIGURE 6
(a) GCD curve for NGP0.2, NGP0.3, NGP0.4 and NGP0.5 at 1 A/g **(b–e)** GCD curve for NGP0.2, NGP0.3, NGP0.4 and NGP0.5 at different current density.

TABLE 5 Specific capacitance of NGP composite at current density of 1 A/g.

Material	Specific capacitance (F/g)
NGP0.2	304.95
NGP0.3	447.23
NGP0.4	**668.87**
NGP0.5	94.51

The bold value represents optimized NGP composite with maximum specific capacitance.

TABLE 6 Variation of Specific capacitance, Energy density and Power density for NGP0.4 at different current density.

Current density (A/g)	Specific capacitance (F/g)	Energy density (W h/kg)	Power density (W/kg)
1	668.87	75.25	450.01
2	603.64	67.91	900.00
3	553.23	62.24	1,350.03
4	509.24	57.29	1800.00

The bold value represents optimized NGP composite with maximum specific capacitance.

2022). The specific surface area calculated using multi-point BET theory is 68.936 m^2/g for NGP composite while it is 85.896 m^2/g and 82.071 m^2/g for g-C_3N_4 and PPy respectively. The lower surface area of NGP composite than its individual constituents is likely due to its reduced pore volume. In the composite Nb_2O_5 effectively covers the smallest pores, thus decreasing the accessible surface area (Mosch et al., 2016). This observation aligns well with the FESEM images where Nb_2O_5 nanoparticles has acquired the surface of g-C_3N_4 and forming a network with PPy. Some particles of Nb_2O_5 occlude the pores of PPy, further contributing to the reduced surface area. The distribution of pore volume and pore diameter is detailed in Table 2. This data underscores the synergistic interaction within the composite, which impacts its overall porosity and surface characteristics.

To identify the reaction mechanism of charge storage, CV was performed in a potential window from −0.2V to 0.7 V for NGP0.2, NGP0.3, NGP0.4 and NGP0.5 at 10 mV/s is shown in Figure 5a. It was observed that NGP0.4 has the highest area under CV curve and hence the specific capacitance. The value of specific capacitance for all the composites was calculated using Equation 1 and is tabulated in Table 3. To further study about the kinetics of reaction, CV was recorded at different scan rates varying from 2 mV/s to 100 mV/s demonstrated in Figures 5b–e. It was observed that on increasing the scan rate, area under CV curve increases which might be due to the increase in capacitive current because of the faster storing and releasing of charge at the electrode surface. But the value of specific capacitance, as depicted in Table 4, decreases due to the fast reaction kinetics, the ions have less time to diffuse into the deeper pores of electrode material leading to incomplete utilization of electrode material. Thus, at high scan rates, specific capacitance which is the amount of charge stored

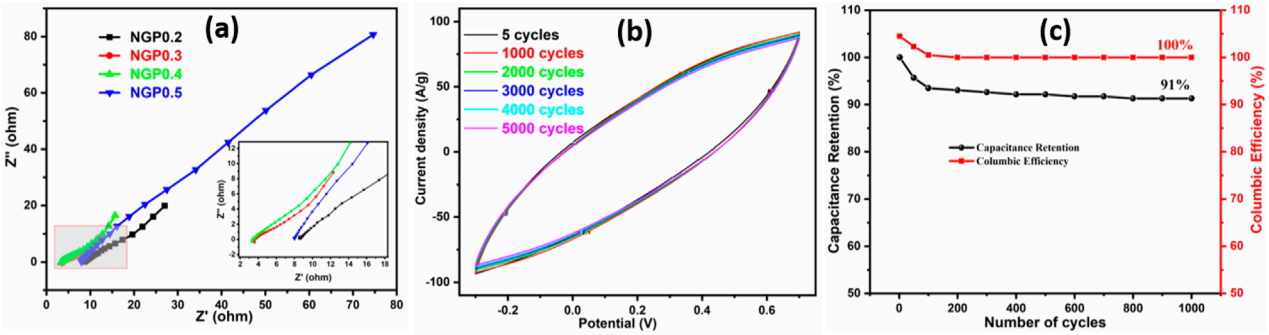

FIGURE 7
(a) Nyquist plot for NGP0.2, NGP0.3, NGP0.4 and NGP0.5 in the frequency range 0.1 Hz–100 KHz (inset) zoom view of Nyquist plot at higher frequency **(b)** CV curve of NGP0.4 composite after different cycles **(c)** Capacitance retention and columbic efficiency after 1000 GCD cycles.

TABLE 7 Comparison of energy density and power density of NGP0.4 composite with previously reported materials in three-electrode system.

Electrode material	Energy density (W h kg^{-1})	Power density (W kg^{-1})	References
PANI/AC/CuF	49.66	300.06	Pandey, Verma, and Verma (2022)
NiO/Gr/PPy	33.71	250.00	Golkhatmi et al. (2021)
PPy/GA	73.00	599.00	Ullah et al. (2022)
$CuMnO_2$/g-C_3N_4	12.50	300.00	Siwal et al. (2020)
Fe_2O_3/rGO/PPy	19.50	100.00	Moyseowicz et al. (2017)
g-C_3N_4/PPy	86.00	300.00	Arora et al. (2022b)
Ag-$NiAl_2O_4$/g-C_3N_4	27.00	187.28	Irshad et al. (2023)
Nb_2O_5/g-C_3N_4/PPy	**75.25**	**450.01**	This work

The bold value represents optimized NGP composite with maximum specific capacitance.

per unit mass decreases because the response is more controlled by the kinetics of electrode process rather than by capacitive behavior (Pan et al., 2024).

To further study about the charge storing capability of electrode material, GCD was performed for NGP0.2, NGP0.3, NGP0.4 and NGP0.5 at 1 A/g as shown in Figure 6a. The specific capacitance, energy density and power density were calculated using Equations 2-4 respectively and is shown in Table 5. It was observed that NGP0.4 has the highest value of specific capacitance among all the NGP composites which is consistent with the CV measurements. The rate capability of NGP composites was studied by varying the current density and is shown in Figures 6b–e. On increasing the current density, the specific capacitance and hence the energy density decreased as shown in Table 6 because of the incomplete charging-discharging of electrode material in limited time frame.

To analyze the solution resistance and charge transfer resistance, Electrochemical Impedance Spectroscopy (EIS) was performed in the frequency range from 0.1 Hz to 10^5 Hz. Figure 7a demonstrates the Nyquist plot of NGP0.2, NGP0.3, NGP0.4 and NGP0.5. In the high frequency region, the point from where EIS plot starts denotes the solution resistance (Laschuk et al., 2021). It can be observed that NGP0.4 has the lowest solution resistance, thus validating the CV and GCD measurements which demonstrate its high specific capacitance than other composites. Further, the negligible presence of semi circle in high frequency region demonstrates the supercapacitive behavior of materials. The cyclic stability of the composite was evaluated by performing 5000 CV cycles and 1000 GCD cycles as shown in Figures 7b,c respectively. It was observed that after 5,000 cycles, 95% of the capacitance was retained from CV cycles and 91% capacitance was retained after 1000 GCD cycles. The difference in capacitance retention from CV and GCD cycles might be attributed to the extent of electrode-electrolyte interactions at higher scan rates, CV with its faster scan rates, might not allow sufficient time for these interactions to fully manifest, potentially demonstrating higher capacitance retention than GCD (Khan et al., 2023). In order to demonstrate the superiority of this work, the energy density of NGP0.4 composite with other previously reported materials is compared in Table 7.

Conclusion

In summary, the Nb_2O_5/g-C_3N_4/PPy (NGP) composite was synthesized via a facile in-situ polymerization reaction with systematic variation in the amount of niobium pentoxide. The successful synthesis of composites was confirmed through XRD pattern which exhibited increased intensity of Nb_2O_5 peaks corresponding to its higher content. The synthesized material displayed a spongy globular morphology which facilitated the faster ion transport and the specific surface area was evaluated from multi

point BET theory and found to be 68.936 m^2/g. Electrochemical measurements revealed a specific capacitance of 1,290.15 F/g at 2 mV/s from CV and 668.87 F/g at 1 A/g as measured with GCD testing. The electrode was further subjected to 5000 CV cycles and 1000 GCD cycles, revealing a capacitance retention of 95% and 91%, respectively. The energy density derived from GCD data was found to be 75.25 W h/kg at a power density of 450.01 W/kg underscoring the capability of this material to be used in future Supercapacitor applications.

Data availability statement

The original contributions presented in the study are included in the article/supplementary material, further inquiries can be directed to the corresponding author.

Author contributions

Manisha: Data curation, Formal Analysis, Investigation, Methodology, Validation, Visualization, Writing–original draft, Writing–review and editing. MQ: Data curation, Methodology, Formal Analysis, Visualization, Writing–review and editing. MD: Data curation, Methodology, Writing–original draft. SL: Resources, Supervision, Validation, Writing–review and editing. HK: Resources, Supervision, Validation, Writing–review and editing. AS: Conceptualization, Funding acquisition, Resources, Supervision, Writing–review and editing.

Funding

The author(s) declare that no financial support was received for the research, authorship, and/or publication of this article.

Acknowledgments

Manisha acknowledges the Council of Scientific and Industrial Research (CSIR) for providing Senior Research Fellowship (Ref. No. 16/06/2019(i) EU-V). Mohammad Taqi Qaeemy acknowledges the Indian Council for Cultural Relations (ICCR) for providing scholarships (Ref. No. MP9471882610549). AS is highly thankful to Anusandhan National Research foundation (ANRF), Department of Science and Technology (DST), Government of India for providing research funding under the SERB University Research Excellence (SURE) scheme (File No. SUR/2022/004191).

Conflict of interest

The authors declare that the research was conducted in the absence of any commercial or financial relationships that could be construed as a potential conflict of interest.

Generative AI statement

The author(s) declare that no Generative AI was used in the creation of this manuscript.

Publisher's note

References

Arora, R., Nehra, S. P., and Lata, S. (2022a). Trio obtainment through polypyrrole insertions in argentum/graphitic carbon nitride for accelerating super-capacitive energy parameters. *J. Energy Storage* 56 (PA), 105879. doi:10.1016/j.est.2022.105879

Arora, R., Pal, S., and Suman, N. (2022b). In - situ composited g - C 3 N 4/polypyrrole nanomaterial applied as energy - storing electrode with ameliorated super - capacitive performance. *Environ. Sci. Pollut. Res.*, 0123456789. doi:10.1007/s11356-022-21777-8

Choudhary, R. B., Ansari, S., and Purty, B. (2020). Robust electrochemical performance of polypyrrole (PPy) and polyindole (PIn) based hybrid electrode materials for supercapacitor application: a review. *J. Energy Storage* 29 (October 2019), 101302. doi:10.1016/j.est.2020.101302

Dhanda, M., Arora, R., Ahlawat, S., Nehra, S. P., and Lata, S. (2022a). Electrolyte as a panacea to contemporary scientific world of super-capacitive energy: a condense report. *J. Energy Storage* 52 (PA), 104740. doi:10.1016/j.est.2022.104740

Dhanda, M., Arora, R., Saini, M., Nehra, S. P., and Lata, S. (2022b). Prolific intercalation of VO2 (D)/Polypyrrole/g-C3N4 as an energy storing electrode with remarkable capacitance. *New J. Chem.* 46, 14251–14266. doi:10.1039/d2nj02401b

Dhanda, M., Nehra, S. P., and Lata, S. (2022c). The amalgamation of G-C3N4 and VO2 (D) as a facile electrode for enhanced storage of energy. *Synth. Met.* 286 (January), 117046. doi:10.1016/j.synthmet.2022.117046

Golkhatmi, S. Z., Sedghi, A., Miankushki, H. N., and Khalaj, M. (2021). Structural properties and supercapacitive performance evaluation of the nickel oxide/graphene/polypyrrole hybrid ternary nanocomposite in aqueous and organic electrolytes. *Energy* 214, 118950. doi:10.1016/j.energy.2020.118950

Hu, Z., He, Q., Liu, Z., Liu, X., Qin, M., Wen, Bo, et al. (2020). Facile Formation of tetragonal-Nb2O5 microspheres for high-rate and stable lithium storage with high areal capacity. *Sci. Bull.* 65 (14), 1154–1162. doi:10.1016/j.scib.2020.04.011

Huan, Z., Sun, C., and Ge, M. (2024). Progress in profitable Fe-based flow batteries for broad-scale energy storage. *WIREs Energy Environ.* 13 (6). doi:10.1002/wene.541

Huang, Y., Li, H., Wang, Z., Zhu, M., Pei, Z., Qi, X., et al. (2016). Nanostructured polypyrrole as a flexible electrode material of supercapacitor. *Nano Energy* 22, 422–438. doi:10.1016/j.nanoen.2016.02.047

Irshad, A., Somaily, H. H., Zulfiqar, S., Warsi, M. F., Imran Din, M., Chaudhary, K., et al. (2023). Silver doped NiAl2O4 nanoplates anchored onto the 2D graphitic carbon nitride sheets for high-performance supercapacitor applications. *J. Alloys Compd.* 934, 167705. doi:10.1016/j.jallcom.2022.167705

Ishaq, S., Moussa, M., Kanwal, F., Ehsan, M., Saleem, M., Truc, N. V., et al. (2019). Facile synthesis of ternary graphene nanocomposites with doped metal oxide and conductive polymers as electrode materials for high performance supercapacitors. *Sci. Rep.* 9 (1), 5974. doi:10.1038/s41598-019-41939-y

Jhanjhariya, N., and Lata, S. (2024). Potential window optimization to upgrade the performance of the designed triad MoS2/MWCNT/PPy as an asymmetric supercapacitor device. *J. Energy Storage* 82 (December 2023), 110577. doi:10.1016/j.est.2024.110577

Khan, R., Muhammad Afzal, A., Hussain, Z., Iqbal, M. W., Imran, M., Waris, M. H., et al. (2023). MnNbS/Polyaniline composite-based electrode material for high-performance energy storage hybrid supercapacitor device. *Phys. Status Solidi (a)* 220 (15). doi:10.1002/pssa.202300200

Laschuk, N. O., Bradley Easton, E., and Zenkina, O. V. (2021). Reducing the resistance for the use of electrochemical impedance spectroscopy analysis in materials chemistry. *RSC Adv.* 11 (45), 27925–27936. doi:10.1039/d1ra03785d

Li, S., Xu, Q., Uchaker, E., Cao, Xi, and Cao, G. (2016). Comparison of amorphous, pseudohexagonal and orthorhombic Nb2O5 for high-rate lithium ion insertion. *CrystEngComm* 18 (14), 2532–2540. doi:10.1039/c5ce02069g

Lim, E., Kim, H., Jo, C., Chun, J., Ku, K., Kim, S., et al. (2014). Advanced hybrid supercapacitor based on a mesoporous niobium pentoxide/carbon as high-performance anode. *ACS Nano* 8 (9), 8968–8978. doi:10.1021/nn501972w

Lü, H., Wang, H., Yang, L., Zhou, Y., Xu, L., Hui, Ni, et al. (2022). A sensitive electrochemical sensor based on metal cobalt wrapped conducting polymer polypyrrole nanocone arrays for the assay of nitrite. *Microchim. Acta* 189 (1), 26–29. doi:10.1007/s00604-021-05131-2

Manisha, M. D., Arora, R., Sudharshan Reddy, A., Lata, S., Sharma, A., and Sharma, A. (2023). Coalescing of lanthanum oxide and PPy @graphitic carbon nitride to achieve ultrahigh energy density electrode material for supercapacitors applications. *J. Alloys Compd.* 955, 169738. doi:10.1016/j.jallcom.2023.169738

Manisha, M. D., Panwar, V., Lata, S., Kumar, H., Sharma, A., and Sharma, A. (2025). Exploring the effect of magnesium oxide on electrochemical properties of polypyrrole encapsulated on graphitic carbon nitride for supercapacitors applications. *J. Energy Storage* 106 (November 2024), 114698. doi:10.1016/j.est.2024.114698

Mao, Y., Xie, J., Liu, H., and Hu, W. (2021). Hierarchical core-shell Ag@Ni(OH)2@PPy nanowire electrode for ultrahigh energy density asymmetric supercapacitor. *Chem. Eng. J.* 405 (August 2020), 126984. doi:10.1016/j.cej.2020.126984

Moreno, R., Pinheiro, A., and Oliveira, H. P.De (2020). Carbon dots reinforced polypyrrole/graphene nanoplatelets on fl exible eggshell membranes as electrodes of all-solid fl exible supercapacitors. *J. Energy Storage* 28 (December 2019), 101284. doi:10.1016/j.est.2020.101284

Mosch, H. L. K. S., Akintola, O., Plass, W., Höppener, S., Schubert, U. S., and Anna, I. (2016). Specific surface versus electrochemically active area of the carbon/polypyrrole capacitor: correlation of ion dynamics studied by an electrochemical quartz crystal microbalance with BET surface. *Langmuir* 32 (18), 4440–4449. doi:10.1021/acs.langmuir.6b00523

Moyseowicz, A., Śliwak, A., Miniach, E., and Gryglewicz, G. (2017). Polypyrrole/iron oxide/reduced graphene oxide ternary composite as a binderless electrode material with high cyclic stability for supercapacitors. *Compos. Part B Eng.* 109, 23–29. doi:10.1016/j.compositesb.2016.10.036

Murugan, M., Kumar, R. M., Ali, A., Alghamdi, A., and Jayavel, R. (2016). Facile hydrothermal preparation of niobium pentaoxide decorated reduced graphene oxide nanocomposites for supercapacitor applications. *Chem. Phys. Lett.* 650, 35–40. doi:10.1016/j.cplett.2016.02.059

Mustaqeem, M., Naikoo, G. A., Yarmohammadi, M., Pedram, M. Z., Pourfarzad, H., Dar, R. A., et al. (2022). Rational design of metal oxide based electrode materials for high performance supercapacitors – a review. *J. Energy Storage* 55 (July), 105419. doi:10.1016/j.est.2022.105419

Pan, H., Jiao, X., Zhang, W., Fan, L., Yuan, Z., and Zhang, C. (2024). Supercapacitor with ultra-high power and energy density enabled by nitrogen/oxygen-doped interconnected hollow carbon nano-onions. *Chem. Eng. J.* 484 (December 2023), 149663. doi:10.1016/j.cej.2024.149663

Pandey, V. K., Verma, S., and Verma, B. (2022). Polyaniline/activated carbon/copper ferrite (PANI/AC/CuF) based ternary composite as an efficient electrode material for supercapacitor. *Chem. Phys. Lett.* 802 (May), 139780. doi:10.1016/j.cplett.2022.139780

Pathak, M., Tatrari, G., Karakoti, M., Pandey, S., Sahu, P. S., Saha, B., et al. (2022). Few layer graphene nanosheets from kinnow peel waste for high-performance supercapacitors: a comparative study with three different electrolytes. *J. Energy Storage* 55 (PC), 105729. doi:10.1016/j.est.2022.105729

Paul, D. R., Sharma, R., Panchal, P., Malik, R., Sharma, A., Tomer, V. K., et al. (2019). Silver doped graphitic carbon nitride for the enhanced photocatalytic activity towards organic dyes. *J. Nanosci. Nanotechnol.* 19 (8), 5241–5248. doi:10.1166/jnn.2019.16838

Paul, D. R., Sharma, R., Singh Rao, V., Panchal, P., Gautam, S., Sharma, A., et al. (2022). Mg/Li@GCN as highly active visible light responding 2D photocatalyst for wastewater remediation application. *Environ. Sci. Pollut. Res.* 30, 98540–98547. doi:10.1007/s11356-022-21203-z

Pore, O. C., Fulari, A. V., Shejwal, R. V., Fulari, V. J., and Lohar, G. M. (2021). Review on recent progress in hydrothermally synthesized MCo 2 O 4/RGO composite for energy storage devices. *Chem. Eng. J.* 426 (April), 131544. doi:10.1016/j.cej.2021.131544

Qin, W., Zhou, N., Wu, C., Xie, M., Sun, H., Guo, Y., et al. (2020). Mini-review on the redox additives in aqueous electrolyte for high performance supercapacitors. *ACS Omega* 5 (8), 3801–3808. doi:10.1021/acsomega.9b04063

Ray, A., and Saruhan, B. (2021). Application of ionic liquids for batteries and supercapacitors. *Materials* 14 (11), 2942. doi:10.3390/ma14112942

Sayed, D. M., Taha, M. M., Ghanem, L. G., El-deab, M. S., and Allam, K. (2020). Hybrid supercapacitors: a simple electrochemical approach to determine optimum potential window and charge balance. *Balance* 480 (September), 229152. doi:10.1016/j.jpowsour.2020.229152

Shen, F., Sun, Z., He, Q., Sun, J., Kaner, R. B., and Shao, Y. (2021). Niobium pentoxide based materials for high rate rechargeable electrochemical energy storage. *Mater. Horizons* 8, 1130–1152. doi:10.1039/D0MH01481H

Shimoga, G., Reddy Palem, R., Choi, D. S., Shin, E. J., Ganesh, P. S., Saratale, G. D., et al. (2021). Polypyrrole-based metal nanocomposite electrode materials for high-performance supercapacitors. *Metals* 11 (6), 905–914. doi:10.3390/met11060905

Siwal, S. S., Zhang, Q., Sun, C., and Thakur, V. K. (2020). Graphitic carbon nitride doped copper–manganese alloy as high–performance electrode material in supercapacitor for energy storage. *Nanomaterials* 10 (1), 2. doi:10.3390/nano10010002

Sun, C., Negro, E., Vezzù, K., Pagot, G., Cavinato, G., Nale, A., et al. (2019). Hybrid inorganic-organic proton-conducting membranes based on SPEEK doped with WO3 nanoparticles for application in vanadium redox flow batteries. *Electrochimica Acta* 309 (June), 311–325. doi:10.1016/j.electacta.2019.03.056

Ullah, R., Khan, N., Khattak, R., Khan, M., Khan, M. S., and Ali, O. M. (2022). Preparation of electrochemical supercapacitor based on polypyrrole/gum Arabic composites. *Polymers* 14 (2), 242. doi:10.3390/polym14020242

Vandana, M., Veeresh, S., Ganesh, H., Nagaraju, Y. S., Vijeth, H., Basappa, M., et al. (2022). Graphene oxide decorated SnO2 quantum dots/polypyrrole ternary composites towards symmetric supercapacitor application. *J. Energy Storage* 46 (January), 103904. doi:10.1016/j.est.2021.103904

Vicentini, R., Nunes, W., Freitas, B. G. A., Da, L. M., Marcelo, D., Cesar, R., et al. (2019). Niobium pentoxide nanoparticles @ multi-walled carbon nanotubes and activated carbon composite material as electrodes for electrochemical capacitors. *Energy Storage Mater.* 22 (August), 311–322. doi:10.1016/j.ensm.2019.08.007

Zhang, X., Wang, J., Liu, J., Wu, Ji, Chen, H., and Bi, H. (2017). Design and preparation of a ternary composite of graphene oxide/carbon dots/polypyrrole for supercapacitor application: importance and unique role of carbon dots. *Carbon* 115, 134–146. doi:10.1016/j.carbon.2017.01.005